Capillary imbibition of shear-thinning fluids: From Lucas-Washburn to oscillatory regimes

Camille Steinik
Mines Saint-Etienne, University of Lyon, CNRS, UMR 5307 LGF, Centre SPIN, F-42023 Saint-Etienne, France

Davide Picchi*
Università degli Studi di Brescia, Department of Mechanical and Industrial Engineering, via Branze 38, Brescia 25123, Italy

Gianluca Lavalle
Mines Saint-Etienne, University of Lyon, CNRS, UMR 5307 LGF, Centre SPIN, F-42023 Saint-Etienne, France

Pietro Poesio
Università degli Studi di Brescia, Department of Mechanical and Industrial Engineering, via Branze 38, Brescia 25123, Italy

(Received 13 June 2023; accepted 24 January 2024; published 28 February 2024)

The study of capillary imbibition has ramifications in many fields, such as energy, biology, process industry, and subsurface flows. Although the capillary rise of Newtonian liquids has been the subject of several studies since the seminal works of Lucas (1918) and Washburn (1921), its generalization to the case of non-Newtonian fluids is still an open question. To fill this gap, starting from first principles, we derive a transient one-dimensional model describing the rising dynamics of shear-thinning fluid, whose viscosity is described by the Ellis viscosity model. Our model identifies the scaling for the different imbibition regimes accounting for the interplay of inertial, gravity, and viscous non-Newtonian effects (i.e., the zero-shear-rate and the shear-thinning behavior). Specifically, the rising dynamics is described by the interplay of three dimensionless parameters: the Richardson number (i.e., the ratio between potential and kinetic energies), the Ellis number (i.e., the ratio between the characteristic shear-stress of the fluid and gravity), and the shear-thinning index which quantify the degree of shear-thinning of the fluid. At early times the system follows a universal inertial regime, followed by two possible limiting regimes, i.e., the classical Lucas-Washburn and the oscillatory regimes. The competition between the governing dimensionless numbers dictates the transition between the two. We show that when the viscous effect dominates over inertia, the identification of a (time-dependent) scaling law for the effective viscosity leads to a generalization of the Lucas-Washburn theory and the rescaled trajectories toward equilibrium collapse over the classical $1/2$ scaling law. On the contrary, when inertia dominates the later stage of the imbibition, the filling length oscillates around the equilibrium. By means of linear control theory, we discuss the physical mechanisms that lead to such oscillating behavior and map the different regimes in terms of the governing dimensionless parameters.

DOI: 10.1103/PhysRevFluids.9.023305

*davide.picchi@unibs.it

I. INTRODUCTION

The study of capillary imbibition finds applications in many fields, such as energy, biology [1], food industry [2], and soil remediation [3]. The rise of a liquid inside a capillary has been a classical problem in fluid mechanics since the seminal work of Lucas [4] and Washburn [5]. Specifically, in regimes where viscous and capillary forces compete, the imbibition of a Newtonian fluid is described by the well-known Lucas-Washburn law

$$\hat{h} = \left(\frac{R\sigma \cos(\theta)}{2\mu} \hat{t} \right)^{1/2}, \tag{1}$$

where $\hat{h}$ is the height of the meniscus, $\hat{t}$ the time, R the radius of the capillary, σ the surface tension, θ the static contact angle, and μ the dynamic viscosity, respectively. Thanks to its simplicity, the Lucas-Washburn law is widely used [6–8] although few inconsistencies between the theory and the experimental rate of the rise have been reported in [8,9]. So far, many attempts have been made to improve the description of the imbibition process of Newtonian fluids by taking into account the inertial effects [10,11], the impact of the dynamic angle on the transient dynamics [9,12,13], and the role of the displaced fluid [14–16] or the tube geometry [17].

Although the imbibition dynamics has been the subject of several studies, the case where the fluid exhibits a non-Newtonian behavior is much less understood. In many scenarios, the working fluid exhibits a shear-thinning behavior (e.g., biological fluids, polymers, suspensions) and its viscosity is a function of the imposed shear-rate, see Bird *et al.* [18]. The viscosity decreases following a power-law behavior only at intermediate shear-rates, while it approaches a constant value at low and high shear rates: the zero-shear-rate and the infinity-shear rate limits, respectively. Such limiting behaviors, are often ignored in the mathematical description of the imbibition dynamics.

Among all the works focusing on the capillary rise of non-Newtonian fluid, many authors considered the idealized power-law viscosity model, see Refs. [19–23], regardless of its physical inconsistencies. The power-law model is singular in the limit of zero shear rate and it is incapable to represent the viscosity plateau either at high or low shear rates, leading to large errors in predicting integral variables, see, for example, Refs. [24–27].

To fill those gaps, our goal is to develop a model capable of describing the entire imbibition dynamics for a realistic shear-thinning fluid accounting for the evolution of the effective viscosity at low shear-rates. We aim at clarifying the competition between inertial, viscous and non-Newtonian (i.e., the zero-shear-rate and the shear-thinning behaviors) effects during the entire imbibition dynamics.

To this aim, we propose a lubrication approximation for the capillary rise of a shear-thinning fluid whose viscosity is described by the Ellis viscosity model [28], derived from the energy balance of the system. Specifically, the use of the Ellis rheological model is convenient since, differently from the Carreau viscosity model [29], it allows for an analytical calculation of the velocity profile in a straight capillary. The capillary rise obeys a nonlinear second-order differential equation where the governing parameters are the Richardson number, which weights potential to kinetic energy, the Ellis number, which accounts for the interplay of zero-shear rate and shear-thinning effects, and the degree of shear thinning of the non-Newtonian fluid. Our model generalizes the capillary rise to shear-thinning fluids by identification of the relevant scaling relations at the different stages of the imbibition. An initial inertial regime is followed by the classical Lucas-Washburn or the oscillatory regimes, depending on the competition between the governing dimensionless numbers. After discussing the mechanism that leads to an oscillating regime using linear control theory, we discuss to which extent the use of the power-law viscosity model can be legitimized in this context.

The results shed light on the imbibition in the context of inelastic shear-thinning fluids and may inspire more sophisticated models for the imbibition process in more complex materials.

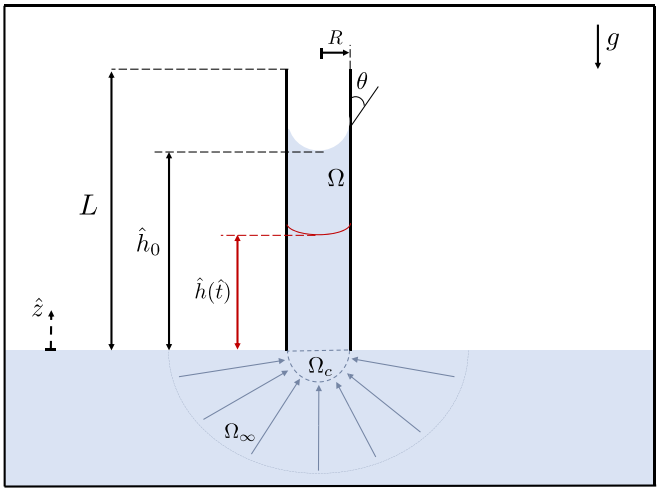

FIG. 1. Sketch of the considered problem: the capillary rise of a shear-thinning fluid in a cylindrical tube of radius R. Note that air viscosity and density are negligible if compared to the liquid ones.

II. THEORETICAL DERIVATION

A. Problem formulation

We consider the rise of a shear-thinning fluid of density ρ in a cylindrical capillary tube of radius R under the effect of gravity and capillary forces; see Fig. 1. The radius is assumed to be much smaller compared to the tube length, $R \ll L$. The bottom reservoir is assumed to be sufficiently big so that only the fluid in the proximity of the tube entrance is affected by the imbibition, and both air and the liquid sufficiently far from the capillary are at rest. For the sake of simplicity, we assume that the configuration depicted in Fig. 1 is a closed system and that air viscosity and density are negligible. The tube walls are assumed to be smooth, neglecting the dissipation due to superficial roughness [30].

The fluid is an incompressible generalized Newtonian fluid whose effective viscosity, μ, is described by the Ellis model [18,28]

$$\mu = \frac{\mu_0}{1 + (\hat{\tau}/\tau_{1/2})^{\alpha-1}}, \tag{2}$$

where $\hat{\tau} = \sqrt{1/2(\hat{\boldsymbol{\tau}} : \hat{\boldsymbol{\tau}})}$ is the effective shear-stress (or the magnitude of the shear stress tensor $\hat{\boldsymbol{\tau}}$). Equation (2) reduces to a Newtonian viscosity μ_0, the zero-shear-rate viscosity, in the limit of small shear rates while, at intermediate shear rates, the index α controls the decreasing of the viscosity. Specifically, the shear-thinning region becomes more significant when α is high ($\alpha \geqslant 1$). The parameter $\tau_{1/2}$ controls the onset of the shear-thinning effect representing the effective shear stress at which the viscosity is 50% of the zero-shear-rate viscosity. When $\tau_{1/2}$ is large, the Newtonian plateau extends up to high shear rates and vice versa. The Ellis model describes well the viscosity of many aqueous solutions where the typical values of the rheological constants are in the range $\alpha \in (1, 3)$ [−] and $\tau_{1/2} = \mathcal{O}(10^{-3} - 10)$ [Pa], and the viscosity of many polymers, where $\alpha \in (1, 4)$ [−] and $\tau_{1/2} = \mathcal{O}(1 - 10)$ [Pa]; see Bird *et al.* [18]. In the following, we will restrict our attention to fluids where the effect of the infinite-shear-rate viscosity can be neglected as in the case of many concentrated polymer solutions [18,31].

Aimed at deriving an evolution equation for the capillary filling, we adopt a one-dimensional representation of the process using the lubrication approximation. We assume laminar flow and, since $R \ll L$ and given the symmetry, we neglect the azimuthal component of the velocity, i.e., the

flow is considered unidirectional and at each cross section, the velocity is only a function of the radial coordinate and time $\hat{\boldsymbol{u}} = \hat{u}(\hat{r}, \hat{t})\boldsymbol{k}$ (where $\boldsymbol{k}$ is the unit vector in the axial direction). Thus, $\hat{u}(\hat{r}, \hat{t})$ is the fully developed velocity profile in a straight tube for an Ellis fluid (see Bird *et al.* [18]) given by

$$\hat{u}(\hat{r}, \hat{t}) = \frac{\hat{P}R^2}{4\mu_0}\left\{\left[\left(\frac{\hat{r}}{R}\right)^2 - 1\right] + \frac{2}{\alpha+1}\left(\frac{|\hat{P}|R}{2\tau_{12}}\right)^{\alpha-1}\left[\left(\frac{\hat{r}}{R}\right)^{\alpha+1} - 1\right]\right\}, \tag{3}$$

where $\hat{P}(\hat{z}, \hat{t}) = \partial\hat{p}/\partial\hat{z}$ and $\hat{r} \in [0; R]$. Although the lubrication approximation is not strictly valid at the tube entrance because of the sudden change in geometry [8,9,32], previous works showed that the impact of such entrance effects on the pressure profiles in the axial direction is negligible, see Refs. [33–35]; a discussion on the impact of the boundary layer growth at the tube entrance is provided in Appendix 1. Therefore, we assume that the velocity profile at the tube entrance is flat and equal to the the instantaneous cross-sectional averaged velocity defined as

$$\hat{U}(\hat{t}) = \frac{2}{R^2}\int_0^R \hat{r}\hat{u}(\hat{r}, \hat{t})\,\mathrm{d}\hat{r} = -\frac{\hat{P}R^2}{8\mu_0}\left[1 + \frac{4}{\alpha+3}\left(\frac{|\hat{P}|R}{2\tau_{12}}\right)^{\alpha-1}\right]. \tag{4}$$

In the liquid reservoir the radial velocity is nonzero only in the regions labeled as Ω_c and Ω_∞ in Fig. 1. Specifically, Ω_c is an hemisphere of radius R where we assume that the radial velocity is uniform with norm equal to $u_c(r, t) = \hat{U}(\hat{t})$. This assumption does not ensure the continuity of the velocity at the boundary between the Ω_c and the outer region Ω_∞, but it can be justified in the limit of $L \gg R$. In fact, although in the region Ω_c the velocity field is rather complex, due to the fact that $L \gg R$ the volume of fluid in such region is rather small if compared to volume of the liquid column and the liquid reservoir and, therefore, its contribution is small. In the outer region Ω_∞ the radial flow decays as shown in Szekely *et al.* [8]. By volume conservation between the tube entrance, $\pi R^2\hat{U}(\hat{t})$, and the surface of the hemisphere, $2\pi R^2\hat{u}_\infty(R, \hat{t})$, we get $\hat{u}_\infty(R, \hat{t}) = \hat{U}(\hat{t})/2$. Using the continuity equation from the curved surface of the hemisphere where $\hat{r} = R$ to a generic radial position in Ω_∞ we obtain

$$2\pi R^2\hat{u}_\infty(R, \hat{t}) = 2\pi r^2\hat{u}_\infty(\hat{r}, \hat{t}), \tag{5}$$

and, therefore, the radial velocity profile yields to

$$\hat{u}_\infty(\hat{r}, \hat{t}) = \frac{R^2}{2\hat{r}^2}\hat{U}(\hat{t}), \quad \hat{r} \in \Omega_\infty. \tag{6}$$

B. Energy balance

Aimed at determining the location of the air-fluid interface with time, $\hat{h}(\hat{t})$, we formulate the energy balance for the entire system depicted in Fig. 1. We start from the energy balance for a closed system filled with two immiscible fluids separated by an interface Σ given by Dussan [36],

$$\frac{d}{d\hat{t}}[\hat{\mathcal{E}} + \hat{\mathcal{P}} + \hat{\mathcal{S}}] = \oint_{\partial\hat{\Sigma}} \sigma\boldsymbol{t}\cdot\hat{\boldsymbol{U}}_{cl}\,d\hat{\ell} - \hat{\Phi}, \tag{7}$$

where $\hat{\mathcal{E}}$, $\hat{\mathcal{P}}$, and $\hat{\mathcal{S}}$ are the kinetic, the potential, the surface energy, respectively, whereas $\partial\hat{\Sigma}$ is the wall-interface contact line and $d\hat{\ell}$ is the unit vector on $\partial\hat{\Sigma}$; the surface energy $\hat{\mathcal{S}}$ refers to the interface Σ separating the liquid and the gas. The total energy of the system can vary due to the work done by the contact line [the first integral on the right-hand side of Eq. (7)] and viscous dissipation, $\hat{\Phi}$; $\hat{\boldsymbol{U}}_{cl}$, σ, and $\boldsymbol{t}$ are the velocity of the contact line, the surface tension, and the unit vector normal to $\partial\hat{\Sigma}$ on $\hat{\Sigma}$.

The kinetic energy of the system is given by

$$\hat{\mathcal{E}} = \int_{\Omega} \frac{1}{2}\rho \hat{u}^2 d\hat{V} + \int_{\Omega_c} \frac{1}{2}\rho \hat{u}_c^2 d\hat{V} + \int_{\Omega_\infty} \frac{1}{2}\rho \hat{u}_\infty^2 d\hat{V}. \tag{8}$$

Plugging in the velocity profiles defined in the previous section and recalling that $d\hat{V} = 2\pi r^2 dr$ for Ω_c and Ω_∞, whereas $d\hat{V} = 2\pi \hat{r} d\hat{r} d\hat{h}$ for Ω, we obtain the following expression for the kinetic energy:

$$\hat{\mathcal{E}} = \tfrac{1}{2}\rho\pi R^2 \gamma \hat{h}\hat{U}^2 + \tfrac{1}{3}\rho\pi R^3 \hat{U}^2 + \tfrac{1}{4}\rho\pi R^3 \hat{U}^2, \tag{9}$$

where γ is a shape factor defined as

$$\gamma = \frac{\int_0^R 2\hat{r}\hat{u}^2 d\hat{r}}{R^2\hat{U}^2}. \tag{10}$$

The shape factor accounts for the shape of the velocity profile in the tube. Specifically, for Newtonian fluids the velocity profile is parabolic and $\gamma = 4/3$; for shear-thinning fluids the shape factor dynamically changes with the pressure gradient and the shape factor is a function of the driving force and the fluid rheology, as shown in Appendix 2. The potential energy of the system is given by

$$\hat{\mathcal{P}} = \pi R^2 \int_0^{\hat{h}} \rho g \hat{z} d\hat{z} = \rho g \pi R^2 \frac{\hat{h}^2}{2}. \tag{11}$$

The determination of the surface energy requires information on the dynamical shape of the meniscus during the imbibition. Since we focus on regimes where capillary and viscous forces dominates the meniscus, we assume that its curvature is constant [i.e., a spherical cap which moves at the speed $\hat{U}(\hat{t})$] and its shape is determined by the contact angle between the liquid and the solid. In general, when the triple point moves, the apparent contact angle, θ_a, is different from the static contact angle, θ, and several factors including the speed of the meniscus, small-scale molecular or kinetic effects (see, for example, Ref. [13]) may affect its motion. In this work, we focus only on the macroscopic imbibition of the liquid where the apparent contact angle is primarily determined by viscous effects, and, therefore, the classical Cox-Voinov relation [37,38] holds

$$\theta_a^3 = \theta^3 + \frac{9\mu_0 \hat{U}(\hat{t})}{\sigma} \log \varepsilon, \tag{12}$$

where $\varepsilon = R/\ell_m$ is the ratio between the length scale of the problem, R, and the cutoff length scale ℓ_m below which the continuum description breaks down. The Cox-Voinov relation can be considered a good approximation also for the case of shear-thinning fluids since the impact of the shear-thinning effect on the spreading dynamics is small, as shown by Neogi and Ybarra [39]. Thus, assuming that the air-liquid interface in the outer reservoir is unperturbed, the surface energy in Eq. (7) can be estimated writing the surface area as a function of the tube radius and the contact angle as follows:

$$\hat{\mathcal{S}} = \oint_{\hat{\Sigma}} \sigma d\hat{S} = \frac{2\pi\sigma R^2}{1 + \sin\theta_a}. \tag{13}$$

The flow in the tube is driven by capillary forces and the work done by the contact line in Eq. (7) is given by

$$\oint_{\partial\hat{\Sigma}} \sigma \boldsymbol{t} \cdot \hat{\boldsymbol{U}}_{cl} d\hat{\ell} = 2\pi R\sigma \cos\theta_a \hat{U}, \tag{14}$$

while viscous dissipation in the liquid is estimated as the sum of the dissipation in the liquid column, $\hat{\Phi}_\Omega$, and in the reservoir, $\hat{\Phi}_\infty$,

$$\hat{\Phi} = \hat{\Phi}_\Omega + \hat{\Phi}_\infty, \tag{15}$$

where

$$\hat{\Phi}_\Omega = \int_0^h \int_0^R 2\pi r \mu \left(\frac{\partial \hat{u}}{\partial \hat{r}}\right)^2 d\hat{r} d\hat{z} \quad \text{and} \quad \hat{\Phi}_\infty = \int_R^\infty 4\pi r^2 \mu \left[\left(\frac{\partial \hat{u}_\infty}{\partial \hat{r}}\right)^2 + \left(\frac{\hat{u}_\infty}{\hat{r}}\right)^2\right] d\hat{r}. \tag{16}$$

Recalling that $\hat{\tau}_{rz} = \mu(\partial \hat{u}/\partial \hat{r})$, and plugging the relation between the shear-rate and the shear stress of an Ellis fluid

$$\frac{d\hat{u}}{d\hat{r}} = \frac{\hat{\tau}_{rz}}{\mu_0}\left(1 + \frac{|\hat{\tau}_{rz}|^{\alpha-1}}{\tau_{1/2}^{\alpha-1}}\right), \tag{17}$$

into Eq. (16) we get a general expression for the viscous dissipation of an Ellis fluid

$$\hat{\Phi}_\Omega = \hat{h} \int_0^R 2\pi r \frac{\hat{\tau}_{rz}^2}{\mu_0}\left(1 + \frac{|\hat{\tau}_{rz}|^{\alpha-1}}{\tau_{1/2}^{\alpha-1}}\right) d\hat{r}. \tag{18}$$

Since from the momentum balance in tube we get that $\hat{\tau}_{rz} = \hat{P}\, r/2$, integration of Eq. (18) yields

$$\hat{\Phi}_\Omega = \frac{\pi \hat{P}^2 R^4 \hat{h}}{8\mu_0}\left[1 + \frac{4}{(3+\alpha)}\left(\frac{\hat{P}R}{2\tau_{1/2}}\right)^{\alpha-1}\right]. \tag{19}$$

An expression for the dissipation in the liquid reservoir, $\hat{\Phi}_\infty$, cannot be derived analytically due to the structure of the Ellis viscosity model and it has to be calculated numerically combining Eqs. (16), (6), and (2).

To sum up, combining all the expressions given above and assuming that $\hat{U}(\hat{t}) = \dot{\hat{h}}$, the energy balance, Eq. (7), reads

$$\begin{aligned}\rho \dot{\hat{h}} \hat{h}\left(\gamma \hat{h} + \frac{1}{2}\hat{h}\hat{h}\frac{d\gamma}{d\hat{h}} + \frac{7}{6}R\right) + \frac{1}{2}\rho\gamma \dot{\hat{h}}^3 + \rho g \hat{h}\dot{\hat{h}} - \frac{2\sigma\cos\theta_a}{(1+\sin\theta_a)^2}\frac{d\theta_a}{d\hat{h}}\dot{\hat{h}} \\ = +\frac{2\sigma\cos\theta_a \dot{\hat{h}}}{R} - \frac{\hat{P}^2R^2}{8\mu_0}\left[1 + \frac{4}{(3+\alpha)}\left(\frac{\hat{P}R}{2\tau_{1/2}}\right)^{\alpha-1}\right] - \frac{1}{\pi R^2}\hat{\Phi}_\infty,\end{aligned} \tag{20}$$

where $d\gamma/d\hat{h}$ and $d\theta_a/d\hat{h}$ are calculated from Eqs. (10) and (12), respectively, and $\ddot{\hat{h}} = d\dot{\hat{h}}/dt$.

C. Dimensionless formulation and time evolution of the column height

The problem is made dimensionless introducing the following characteristic scales:

$$h_0 = \frac{2\sigma\cos\theta}{\rho R g}, \quad t_0 = \frac{8\mu_0 h_0}{\rho g R^2}, \quad p_0 = \rho g h_0, \tag{21}$$

where h_0 and t_0 are the characteristic length and time, respectively, in case the capillary force balances with gravity (h_0 is the column height at the equilibrium); p_0 scales with the hydro-static pressure based on h_0. If we introduce the following dimensionless variables

$$h = \frac{\hat{h}}{h_0}, \quad t = \frac{\hat{t}}{t_0}, \quad p = \frac{\hat{p}}{p_0}, \quad P = \frac{\hat{P}}{p_0/h_0}, \tag{22}$$

then we can recast Eq. (20) as follows:

$$\begin{aligned}\frac{1}{\mathrm{Ri}}\left[\dot{h}\ddot{h}\left(\gamma h + \frac{1}{2}h\dot{h}\gamma' + \frac{7}{6}\mathrm{Bo}\right) + \frac{1}{2}\gamma\dot{h}^3\right] + h\dot{h} - \mathrm{Bo}\frac{d\mathcal{S}}{dt} \\ = \frac{\cos\theta_a}{\cos\theta}\dot{h} - hP^2\left[1 + \frac{4}{(3+\alpha)}\left(\frac{P}{2\mathrm{El}}\right)^{\alpha-1}\right] - \mathrm{Bo}\,\Phi_\infty,\end{aligned} \tag{23}$$

TABLE I. List of dimensionless parameters computed in different experimental setups.

	Fluid	α	$\mathcal{O}(\mathrm{Bo})$	$\mathcal{O}(\mathrm{Ri})$	Oscillations	Orientation
Digilov [21]	Power law	1.3	10^{-3}	10^{5}	No	Vertical
Gorthi *et al.* [23]	Power law	1.1	10^{-2}	10^{3}	No	Horizontal
	Power law	1.2	10^{-2}	10^{4}	No	Horizontal
Zhmud *et al.* [16]	Newtonian	–	10^{-2}	10^{-1}	Yes	Vertical

where $\gamma(P(\dot{h}), \mathrm{El}, \alpha)$ and $\gamma' = d\gamma/d\dot{h}$ are the shape factor and its derivative (the full expressions are given in Appendix 2), and $d\mathcal{S}/dt$ is the time derivative of the surface energy given by

$$\frac{d\mathcal{S}}{dt} = \frac{3}{8}\frac{\cos\theta_a}{(1+\sin\theta_a)^2}\frac{\mathrm{Bo}\log\varepsilon}{\left(\theta_0^3 + 9\mathrm{Bo}\cos\theta\,\dot{h}\,\log\varepsilon\right)^{\frac{2}{3}}}\ddot{h}. \tag{24}$$

The evolution equation for the liquid height, Eq. (23), is coupled with the equation for the pressure gradient $P(\dot{h}, \mathrm{El}, \alpha)$ obtained making Eq. (4) dimensionless

$$\dot{h} = -P\left[1 + \frac{4}{\alpha+3}\left(\frac{|P|}{2\mathrm{El}}\right)^{\alpha-1}\right]. \tag{25}$$

The dimensionless parameters appearing in the energy balance are Richardson, Bond, and Ellis numbers defined as

$$\mathrm{Ri} = \frac{gh_0}{(h_0/t_0)^2} = \frac{128\mu_0^2\sigma\cos\theta}{\rho^3 g^2 R^5}, \quad \mathrm{Bo} = \frac{R}{h_0} = \frac{\rho g R^2}{2\sigma\cos\theta}, \quad \mathrm{El} = \frac{\tau_{12}}{R\rho g}. \tag{26}$$

The Richardson number can be interpreted as the ratio between potential and kinetic energy in the liquid column, since the ratio h_0/t_0 is the characteristic speed of the problem. When Ri is high, potential energy dominates over kinetic energy meaning that kinetic terms can be dropped from the left-hand side of Eq. (20). The Bond number is the ratio between buoyancy and surface tension forces or, based on the scaling chosen in this work, the ratio between the tube radius, R, and the characteristic length scale of the imbibition, h_0. The Bond number controls the surface energy terms and the dissipation produced in the liquid reservoirs in Eq. (23). For the sake of physical interpretation, the product $\mathrm{Bo}\cos\theta$ in Eq. (24) is the capillary number, i.e., $Ca = \mu_0(h_0/t_0)/\sigma$. The effect of Bo on the energy balance will be discussed in the next section.

The Ellis number is the ratio between the characteristic shear-stress of the fluid, $\tau_{1/2}$, and the gravitational shear-stress, $R\rho g$. When El is small the shear-thinning effect dominates and the effective viscosity matches that of a power-law fluid with a slope $(1-\alpha)/\alpha$. Instead, when $\mathrm{El} \to \infty$ the onset of the shear-thinning effect is delayed to an infinite shear-rate and Eq. (23) reduces to the Newtonian limit

$$\frac{1}{\mathrm{Ri}}\left[\dot{h}\ddot{h}\left(\frac{4}{3}h + \frac{7}{6}\mathrm{Bo}\right) + \frac{2}{3}\dot{h}^3\right] + h\dot{h} - \mathrm{Bo}\frac{d\mathcal{S}}{dt} = \frac{\cos\theta_a}{\cos\theta}\dot{h} - h\dot{h}^2 - \frac{5}{24}\mathrm{Bo}\,\dot{h}^2, \tag{27}$$

where $\gamma = 4/3$.

1. The small Bond number limit, $\mathbf{Bo} \ll 1$

In this work we are interested in regimes where the meniscus height at the equilibrium is much larger compared to the tube radius, i.e., the Bond number of the problem is small $\mathrm{Bo} = R/h_0 \ll 1$. This limit is representative of many experimental works published in the literature, where the typical Bo is of the order of 10^{-2} as summarized in Table I.

Interestingly, when $\mathrm{Bo} \ll 1$, the energy balance simplifies considerably. If we make Eq. (12) dimensionless

$$\theta_a^3 = \theta^3 + \frac{9\mathrm{Bo}\cos\theta}{8}\dot{h}\log\varepsilon, \tag{28}$$

then we see that when $\mathrm{Bo}\log\varepsilon \ll 1$, the contact angle can be approximated to the static constant angle, $\theta_a \approx \theta$ and we can assume quasistatic conditions similarly to Refs. [11,17,32]. Also, the surface energy term on the left-hand side of Eq. (23) is negligible since $\mathrm{Bo}\, d\mathcal{S}/dt \sim \mathrm{Bo}^2 \log\varepsilon \ll 1$. This means that, in terms of macroscopic imbibition, local variations of the meniscus shape do not affect the time evolution of the column height. In the small Bo limit, we can also neglect the contribution of viscous dissipation in the outer reservoir but not the contribution of flow in the reservoir [i.e., the added mass term, $7/6\,\dot{h}\ddot{h}\,\mathrm{Bo}$, on the left-hand side of Eq. (23)] since it competes with Ri.

To sum up, by making use of Eq. (25) and in the limit of $\mathrm{Bo} \ll 1$, Eq. (23) reduces to

$$\frac{1}{\mathrm{Ri}}\underbrace{\left[\ddot{h}\left(\gamma h + \frac{1}{2}h\dot{h}\gamma' + \frac{7}{6}\mathrm{Bo}\right) + \frac{1}{2}\gamma\dot{h}^2\right]}_{d\mathcal{E}/dt} + \underbrace{h}_{d\mathcal{P}/dt} = 1 + hP, \tag{29}$$

where the energy of the system is the sum of the kinetic and potential contributions and it is dissipated only through the work done by the moving contact line and viscous dissipation in the tube. In the following, we will discuss the imbibition dynamics referring to Eq. (29) coupled with Eq. (25) discussing the impact of the fluid rheology on the imbibition regimes.

When, $\mathrm{El} \to \infty$, Eq. (29) reduces to the Newtonian limit

$$\frac{1}{\mathrm{Ri}}\left(\ddot{h}h + \frac{7}{6}\mathrm{Bo}\,\ddot{h} + \frac{2}{3}\dot{h}^2\right) = 1 - h - h\dot{h}, \tag{30}$$

in agreement with the results obtained by Duarte *et al.* [32].

III. RESULTS AND DISCUSSION IN THE SMALL BOND NUMBER LIMIT

A. The high Richardson number limit: Lucas-Washburn regime

In this section we focus on the imbibition of a shear-thinning fluid in the limit of high Richardson number. When $\mathrm{Ri} \to \infty$, the kinetic term can be dropped from the left-hand side of Eq. (29) and, combining Eqs. (25) and (29) we obtain

$$\dot{h} = -\frac{h-1}{h}\left[1 + \frac{4}{\alpha+3}\left(\frac{1}{2\mathrm{El}}\left|\frac{h-1}{h}\right|\right)^{\alpha-1}\right]. \tag{31}$$

This is a first-order ordinary differential equation for the column height that describes the Lucas-Washburn regime where gravity competes with viscous forces and surface tension only. In this regime, time variations of the potential energy balance the work done by contact line and viscous dissipation in the liquid, and the column height is a function of time, Ellis number and shear-thinning index only, $h = h(t, \mathrm{El}, \alpha)$. Figure 2(a) shows the time evolution of the column height as a function of El obtained by solving Eq. (31) using the solver *ode45* of Matlab with initial condition $h(0) = 0$.

When $\mathrm{El} \to \infty$, the zero-shear-rate effect dominates the fluid behavior and we recover a Newtonian behavior. In this limit, Eq. (31) reduces to $\dot{h} = (1-h)/h$ and admits analytical solution of the type $t = -h - \log(1-h)$. At early and intermediate times where $h \ll 1$, the logarithmic term can be expanded in a Taylor series and the solution follows the classical Lucas-Washburn scaling $h \sim \sqrt{2t}$, as shown in terms of logarithmic slope in the inset of Fig. 2(a). At late time, instead, the liquid column approaches the equilibrium configuration, $h \approx 1$, and the time evolution follows an exponential behavior $h \sim 1 - \exp(t)$.

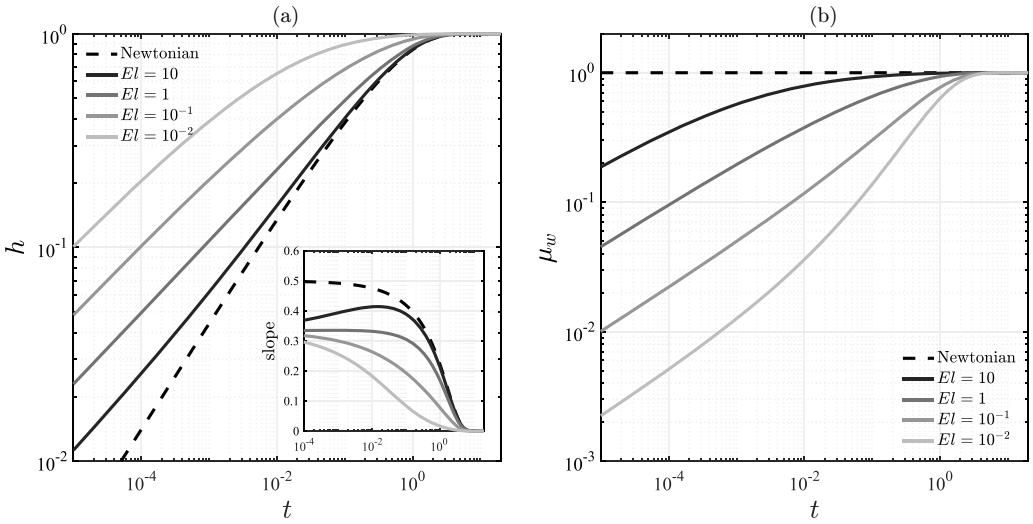

FIG. 2. (a) Time evolution of the column height as a function of the Ellis number for $\alpha = 2$: the inset show the slope of the $h - t$ curve in logarithmic scale; (b) time evolution of the effective viscosity computed at the tube wall as a function of the Ellis number for $\alpha = 2$.

As El decreases, the shear-thinning effect becomes dominant and the time evolution of the column height deviates from the Newtonian limit not following the $1/2$ scaling law. To quantify the shear-thinning effect during the imbibition, we show the evolution of the effective viscosity evaluated at the tube wall in Fig. 2(b). The effective viscosity μ_w is based on the wall-shear stress

$$\mu_w = \frac{1}{1 + (\tau_w/\mathrm{El})^{\alpha-1}}, \quad \text{where} \quad \tau_w = \frac{P}{2}, \tag{32}$$

and it converges to the unity for $\mathrm{El} \to \infty$. For small El, instead, if we plug Eq. (25) into Eq. (32), then we recover an expression for the effective viscosity in the shear-thinning region

$$\mu_w(t, \mathrm{El} \to 0) = \frac{(3+\alpha)^{\frac{1-\alpha}{\alpha}}}{2^{\frac{3(1-\alpha)}{\alpha}}} \left(\frac{|\dot{h}|}{\mathrm{El}}\right)^{\frac{(1-\alpha)}{\alpha}}. \tag{33}$$

Interestingly, the shear-thinning effect is evident only at the early stage of the imbibition, while the later stages are always dominated by the zero-shear rate effect, see Fig. 2(b). This can be explained by inspection of the flow rate relation, Eq. (25), in Fig. 3(a). In the neighbourhood of $P = 0$, the relation between the dimensionless flow rate and the dimensionless pressure gradient is linear, i.e., $\dot{h} = -P + o(P^2)$, and the system's behavior is close to Newtonian. This is confirmed by the trend of the effective viscosity in Fig. 3(b) which reaches the Newtonian limit in the proximity of the equilibrium configuration for $\dot{h} \approx 0$.

The shape of the curves of Fig. 2(a) suggests the existence of a more general scaling law which describes the time evolution of the imbibition. Specifically, the $h - t$ curves can be collapsed if the dimensionless time is rescaled as $t^\star = t/\mu_w$ where μ_w is the dimensionless effective viscosity defined in Eq. (33). In the Newtonian limit, $\mu_w = 1$ and the rescaling is not needed since, in terms of dimensionless variables, the imbibition is described by a unique $h - t$ curve. In Fig. 4(a) we show the rescaled $h - t^\star$ curves for the cases previously discussed observing that the time evolution of the liquid height seems to follow a universal behavior. After the rescaling, in fact, the dynamics of the imbibition is the same as in the Newtonian case and it follows the classical $1/2$ Lucas-Washburn scaling law at intermediate times, as shown in terms of logarithmic slope in the inset of Fig. 4(a). This means that the identification of the following (time-dependent) master curve for

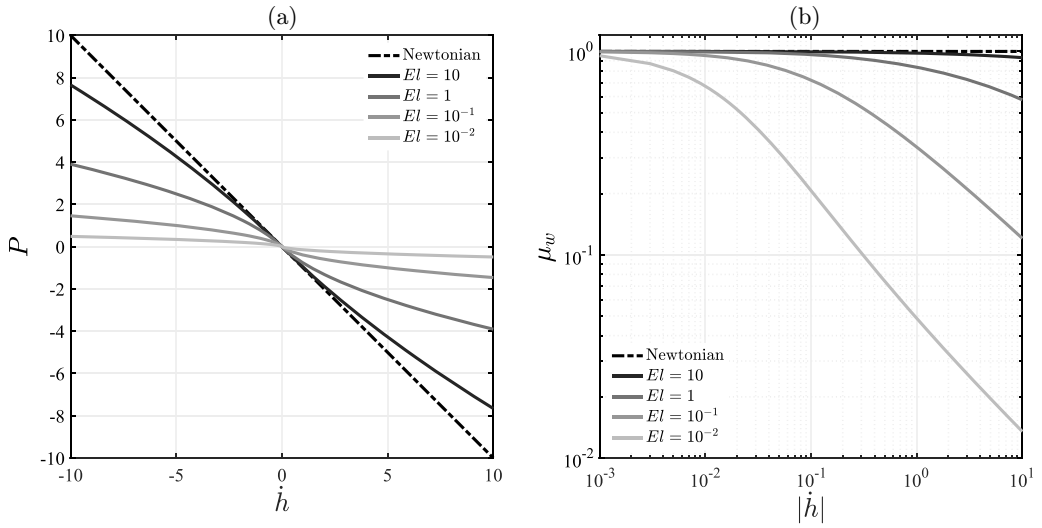

FIG. 3. (a) Evolution of the pressure gradient, P, as a function of the speed of the column, $\dot{h}$, for different El and $\alpha = 2$; (b) evolution of the effective viscosity computed at the tube wall as a function of the speed of the column, $\dot{h}$ for different El and $\alpha = 2$.

the effective viscosity

$$\frac{\mu_w}{\mu_0} = \begin{cases} 1, & \text{if} \quad \text{El} \to \infty, \\ \frac{(3+\alpha)^{\frac{1-\alpha}{\alpha}}}{2^{\frac{3(1-\alpha)}{\alpha}}} \left(\frac{|\dot{h}|}{\text{El}}\right)^{\frac{(1-\alpha)}{\alpha}}, & \text{if} \quad \text{El} \to 0, \end{cases} \tag{34}$$

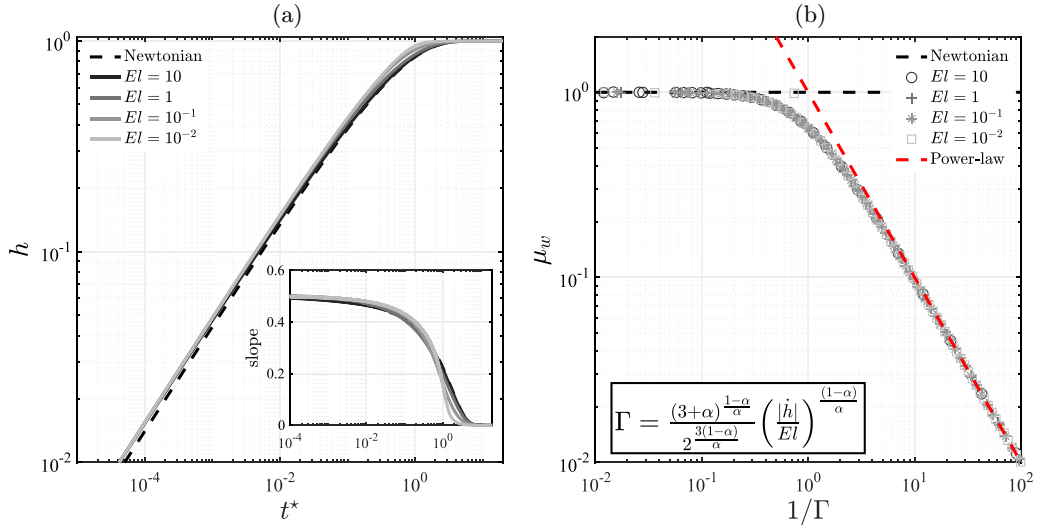

FIG. 4. (a) Rescaled time evolution of the column height for $\alpha = 2$: the inset shows the slope of the $h - t^\star$ curve in logarithmic scale; (b) master curve for the effective viscosity for $\alpha = 2$ as a function of $1/\Gamma$ with Γ defined in Eq. (33) where Γ is the effective viscosity in the El $\to$ 0 limit.

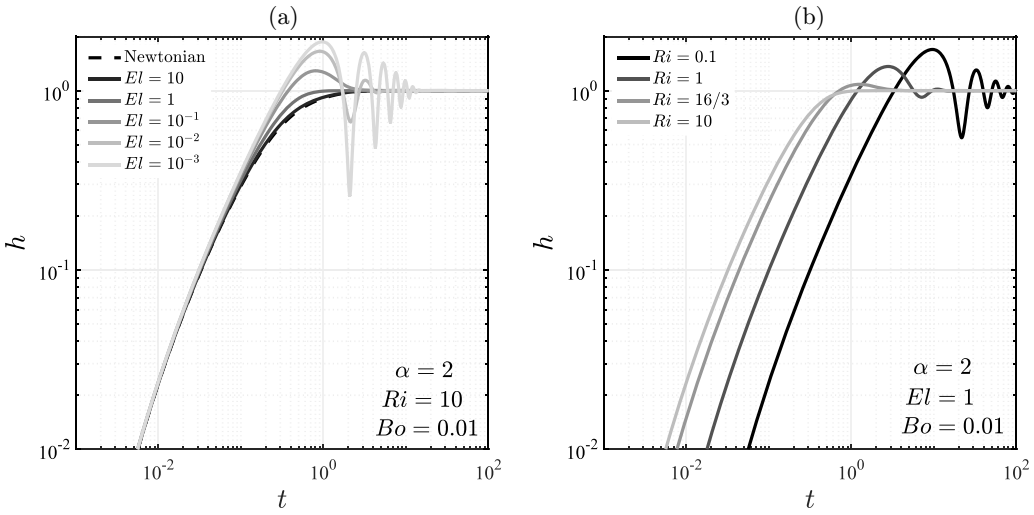

FIG. 5. (a) Time evolution of the column height as a function of the Ellis number. (b) Time evolution of the column height as a function of the Richardson number.

leads to a generalization of the Lucas-Washburn scaling relation to shear-thinning fluids. In other words, the $1/2$ scaling law can be recovered only if the problem is rescaled in terms of the effective viscosity; see Fig. 4(b).

B. Finite Richardson number: Oscillating regime

When the Richardson number is finite, kinetic (or inertial) effects compete with viscous and gravity effects. In this section we will focus on the effect of inertia looking at cases where the boundary layer growth at the tube entrance can be neglected as discussed in Appendix 1. The dynamics is obtained solving Eq. (29) using the solver *ode45* of Matlab with initial conditions $h(0) = \dot{h}(0) = 0$. In this regime, the column height is a function of time, Ellis number, shear-thinning index, as well as of Bond and Richardson numbers, i.e., $h = h(t, \mathrm{El}, \alpha, \mathrm{Bo}, \mathrm{Ri})$.

Figure 5(a) shows the time evolution as a function of El for a case where $\mathrm{Ri} = 10$, $\alpha = 2$, and $\mathrm{Bo} = 0.01$. Differently from the Lucas-Washburn regime, there exists conditions where the filling length oscillates around the equilibrium at the late stage of the imbibition. Specifically, the shear-thinning effect (i.e., at small El) seems to favour the onset of such oscillations. The oscillating behavior is also triggered by the Richardson number, see Fig. 5(b); when Ri is large the time evolution is monotonic while, for small Ri, we observe an overshoot followed by damped oscillations.

Although the existence of an oscillating regime has been observed also for Newtonian fluids [9–11,14,32], here the conditions for triggering the oscillations depends on the fluid rheology. In fact, the oscillations are observed either decreasing El (i.e., conditions where the shear-thinning effect is important) or decreasing Ri (i.e., conditions where kinetic effects in Eq. (29) are important) as shown in Fig. 5.

Aimed at understanding the physical mechanism leading to the oscillating regime, we proceed by studying the linearized system in the Newtonian limit, i.e., $\mathrm{El} \to \infty$. Specifically, Eq. (29) can be seen as a system of first-order differential equations of the form $\dot{\boldsymbol{x}} = \boldsymbol{f}$ where

$$\boldsymbol{x} = \begin{pmatrix} \dot{h} \\ h \end{pmatrix} \quad \text{and} \quad \boldsymbol{f} = \begin{pmatrix} \frac{(1-h+hP)\mathrm{Ri}-1/2\gamma\dot{h}^2}{\gamma h+\frac{1}{2}h\dot{h}\gamma'+\frac{7}{6}\mathrm{Bo}} \\ \dot{h} \end{pmatrix}. \tag{35}$$

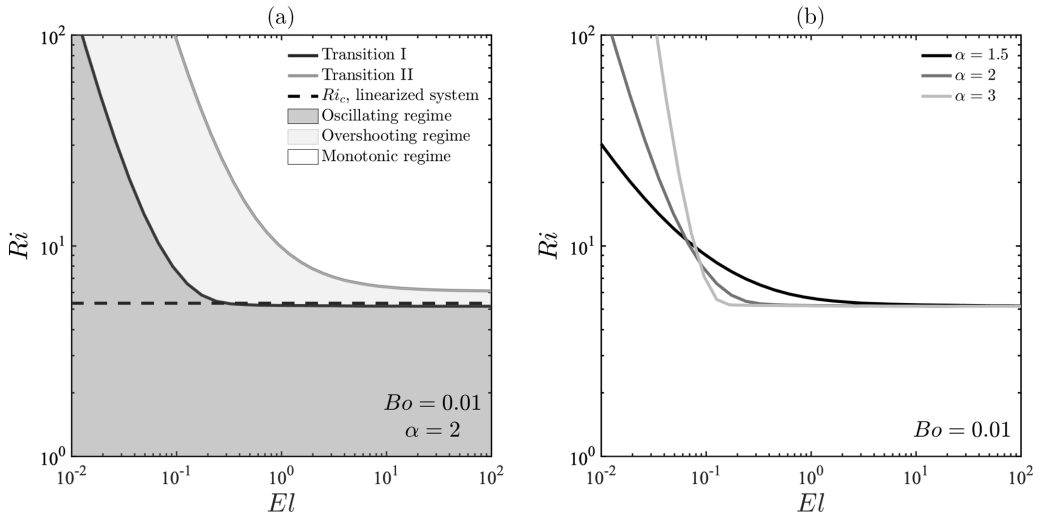

FIG. 6. (a) Map of the system behavior as a function of El and Ri for $\alpha = 2$ and Bo $= 0.01$. (b) Map of the system behavior as a function of El and Ri for different α and Bo $= 0.01$.

If we linearize around the equilibrium configuration $\boldsymbol{x}_0 = (0, 1)^T$ as $\boldsymbol{f}(\boldsymbol{x}) \approx \boldsymbol{f}(\boldsymbol{x}_0) + \boldsymbol{J}(\boldsymbol{x}_0)(\boldsymbol{x} - \boldsymbol{x}_0)$, then the Jacobian in the Newtonian limit (see Appendix 3 for all the details) yields to

$$\boldsymbol{J}(\boldsymbol{x}_0) = \begin{pmatrix} -\frac{3}{4}\mathrm{Ri} & -\frac{3}{4}\mathrm{Ri} \\ 1 & 0 \end{pmatrix}, \tag{36}$$

where its characteristic equation reads

$$\lambda^2 + \tfrac{3}{4}\mathrm{Ri}\lambda + \tfrac{3}{4}\mathrm{Ri} = 0. \tag{37}$$

The system behavior around the equilibrium is dictated by the sign of the discriminant of the the characteristic equation, i.e., $\Delta = \sqrt{3\mathrm{Ri}(3\mathrm{Ri} - 16)/16}$. If Ri $> 16/3$, then the discriminant is positive and both the eigenvalues are negative: In this case, the system does not show an oscillating behavior. Instead, when Ri $< 16/3$ the discriminant is negative meaning that both eigenvalues are complex and conjugate. In this case, the system is stable (the real part of the eigenvalues is positive) and the solution oscillates before reaching the equilibrium configuration. The transition between the two regimes occurs at Ri $= 16/3$ in the limit of Bo $\to 0$.

In Fig. 6(a) the different regimes are mapped as a function of El and Ri. When the Ellis number is sufficiently large the zero-shear-rate effect dominates the system dynamics and the oscillating regime is observed only for Ri $< 16/3$, as predicted in the Newtonian limit. When the shear-thinning effect is important at small El, instead, the oscillating regime extends up to larger Ri. The fact that the shear-thinning effect favours the oscillating behavior can be explained looking at the linearized system in the power-law limit (see Appendix 4). Ignoring the zero-shear-rate effect and assuming a power-law viscosity would predict an unbounded oscillating regime. The effect of the shear-thinning index on the transition between the oscillating and nonoscillating regimes is summarized in Fig. 6(b). Specifically, as the degree of shear-thinning increases ($\alpha \to \infty$) the oscillating regime dominates the low Ellis number region.

The transition between the oscillating and the monotonic regime is not sharp and an intermediate regime characterized by the presence of an overshoot can be identified. Specifically, the overshoot is the maximal liquid height reached by the liquid column exceeding the equilibrium configuration. At some conditions, in fact, the column height overshoots and, then, reaches the equilibrium without showing an oscillating behavior. Figure 7(a) shows the maximal height reached by the liquid column

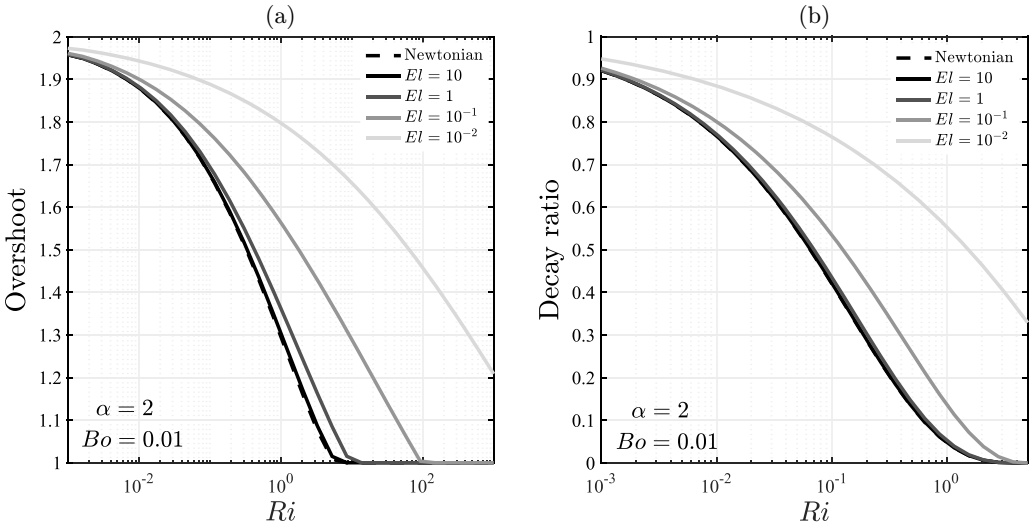

FIG. 7. (a) Overshoot (i.e., the maximal liquid height reached by the liquid column exceeding the equilibrium configuration) as a function of Ri and El for $\alpha = 2$ and Bo $= 0.01$; (b) decay ratio (i.e., the ratio between the height of first oscillation right after the overshoot and the overshoot) as a function of Ri and El for $\alpha = 2$ and Bo $= 0.01$.

as a function of the Ellis and the Richardson numbers. When Ri is large, there is no overshooting and the maximal value coincides with the equilibrium configuration while, at small Ri, the overshoot reaches the limiting values of 2 (note that the results have been shown covering the entire spectrum of Ri only for the sake of completeness, but when Ri is smaller than unity, the results may not be very accurate since the inertial effects at the tube entrance have been neglected; see Appendix 1 for all the details). As expected, the shear-thinning effect favours the overshooting behavior and reduces the decay ratio (defined as the ratio between the height of first oscillation right after the overshoot and the overshoot); see Fig. 7(b). From the physical point of view, the shear-thinning effect reduces the damping of the system since the lower the effective viscosity of the system, the lower the pressure gradient (see Fig. 3 in the limit of El $\ll 1$). This tendency is clear looking at the problem formulation in the power-law limit where the system behaves as an undamped oscillator; see Appendix 4.

IV. CONCLUSION

In this work we studied the filling dynamics of a shear-thinning fluid in a capillary tube. In regimes where inertial effects can be neglected, our analysis identifies a universal scaling law for the effective viscosity that applies to both Newtonian and shear-thinning fluids. Specifically, we generalize the Lucas-Washburn scaling relation to shear-thinning fluids showing that the classical $1/2$ scaling law holds only if an *ad hoc* time-dependent effective viscosity is introduced.

In regimes where inertia competes with viscous and gravity effects, the system shows an oscillating behavior. By means of linear control theory we identified the critical Richardson number responsible for the onset of the oscillations in the Newtonian limit. The shear-thinning effect acts on the system favoring the oscillating behavior both enhancing the overshoot and decreasing the decay ratio. Interestingly, assuming a power-law viscosity neglecting the zero-shear rate effect would lead to nonphysical results suppressing the damping features of the system.

Despite the fact that the motivation of our work is focused on gravity-driven imbibition, our results may inspire more sophisticated models for flow in complex geometries.

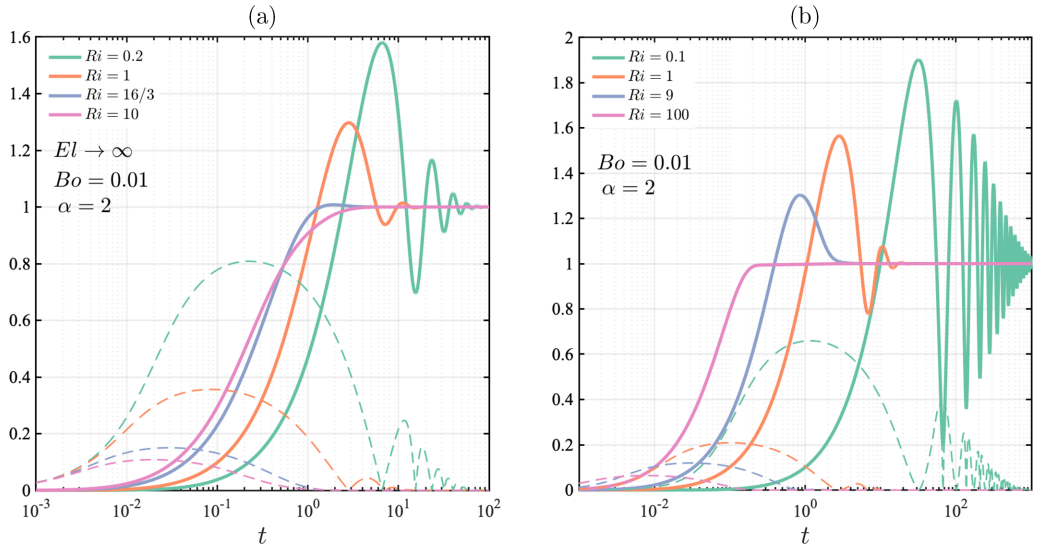

FIG. 8. (a) Evolution of the column speed (solid lines), $\dot{h}$, as a function of time for different Ri when El $\to \infty$ and $\alpha = 2$; Estimate of the entrance length (dashed lines), ℓ, as a function of time for different Ri when El $\to \infty$ and $\alpha = 2$; (b) Evolution of the column speed (solid lines), $\dot{h}$, as a function of time for different Ri when El $= 0.1$ and $\alpha = 2$; Estimate of the entrance length (dashed lines), ℓ, as a function of time for different Ri when El $= 0.1$ and $\alpha = 2$.

ACKNOWLEDGMENTS

This work was supported by the Auvergne-Rhône-Alpes region through the project "MuscaFlow" (Grant No. 21 007147) agreed between Mines Saint-Etienne and Università degli Studi di Brescia.

APPENDIX

1. Boundary-layer growth at the tube entrance

In our model, we neglect the boundary layer growth at the tube entrance, see Sec. II A. This assumption can be justified *a posteriori* by analysis of the entrance length predicted by the classical boundary layer theory; see White [40].

When the zero-shear-rate effect dominates over the shear-thinning effect (i.e., the Newtonian limit El $\to \infty$), the entrance length $\hat{\ell}$ can be estimated using the classical Blausius's theory for Newtonian fluids yielding to

$$\hat{\ell} = \frac{4}{100}\frac{\rho R^2 \dot{\hat{h}}}{\mu_0}. \tag{A1}$$

Following the normalization introduced in Eq. (22), the entrance length normalized with respect to the column height at the equilibrium, $\ell = \hat{\ell}/h_0$, is given by

$$\ell = 0.32\frac{\dot{h}}{\mathrm{Ri}}. \tag{A2}$$

The entrance region is, then, a function of the column speed, $\dot{h}(t)$, and the Richardson number, Ri. Specifically, the column speed is maximal at the early stages of the imbibition and decreases rapidly as the column reaches the equilibrium configuration. Aiming at quantifying the effect of the entrance length, Fig. 8(a) shows the evolution of both the column height and the entrance length calculated by Eq. (A2); ℓ is comparable to $h(t)$ only at very early times, while at later times the column height

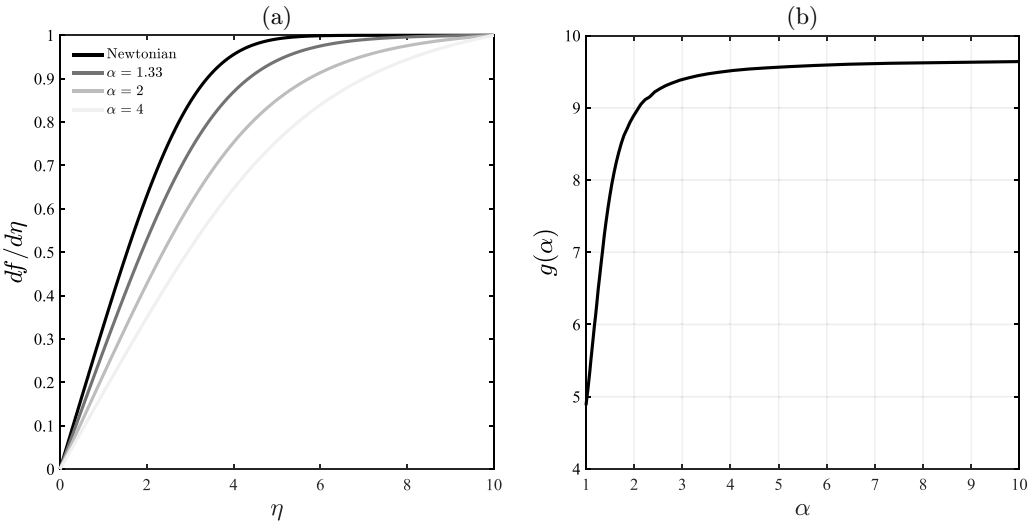

FIG. 9. (a) Evolution of the dimensionless velocity $f'(\eta, \alpha)$ as function of the similarity variable η. (b) Values of the similarity values where the dimensionless velocity equal to 99% of the velocity outside the boundary layer.

is close to equilibrium, the speed is considerably lower, and the importance of the entrance length becomes negligible. Therefore, in the high Ri limit (i.e., the Lucas-Washburn regime, see Sec. III A), the effect of the boundary layer growth is limited to early times, and, overall, its contribution is negligible. In the oscillatory regime (see Sec. III B), instead, neglecting the boundary layer growth dictates a lower bound on the applicability of the model in terms of the Richardson number. In fact, when $\mathrm{Ri} = 16/3$ (i.e., the critical value that determines the transition between the oscillatory and the overshooting regimes, see Sec III B), its effect only impacts early times and $h \gg \ell$ almost during the imbibition. The scenario changes when Ri assumes values lower than unity. In that case, the analysis of Fig. 8(a) suggests that the model should not be applicable since the boundary layer growth would also affect later times of the imbibition.

When the shear-thinning effect dominates (i.e., the Ellis number is small $\mathrm{El} \ll 1$), we estimate the entrance length adapting the boundary layer theory for power-law fluids derived by [41–43] to Ellis fluids approximating the viscosity model given in Eq. (2) with its power-law approximation $\mu = \kappa \dot{\gamma}^{(1-\alpha)/\alpha}$, where $\kappa = \mu_0^{1/\alpha} \tau_{1/2}^{(1-\alpha)/\alpha}$. This choice is motivated by the fact that we are interested only in an estimation of the order of magnitude of the entrance length during the imbibition. The equation describing the boundary layer on a flat plate $\hat{x} - \hat{y}$, see Refs. [41–43], is given by

$$f''' + \frac{\alpha}{\alpha+1} f (f'')^{(2\alpha-1)/\alpha} = 0, \quad \text{with} \quad \eta = \frac{\hat{y}\, \alpha^{\alpha/(\alpha+1)}}{\hat{x}^{\alpha/(\alpha+1)}} \left(\frac{\rho V^{(2\alpha-1)/\alpha}}{\kappa} \right)^{\alpha/(\alpha+1)}, \tag{A3}$$

where η is the similarity variable, V the velocity far from the boundary layer, and $f(\eta, \alpha)$ is a function of the similarity variable and the shear-thinning index only; the local velocity is given by $\hat{u}(\hat{x}, \hat{y})/V = f'(\eta(x, y))$. Equation (A3) subjected to $f(0) = f'(0) = 0$ and $f'(\infty) = 1$ can be solved numerically using the solver *bvp4c* of MatLab to obtain the evolution of the dimensionless velocity $f'(\eta, \alpha)$ as function of the similarity variable. The shear-thinning index affects the velocity profiles as shown in Fig. 9(a).

Using the boundary-layer model, we can calculate the entrance length $\hat{\ell}$ as the length where the boundary layer thickness matches with the tube radius R. Usually, the thickness of the boundary layer is defined as the thickness where the dimensionless velocity equals 99% of the velocity outside the boundary layer. In this case, η_{99} is a function of the shear-thinning index only, namely $\eta_{99} = g(\alpha)$

as plotted in Fig. 9(b) (these results converge to the classical Blausius's theory when $\alpha = 1$). Thus, plugging $\eta = \eta_{99}$ and $\hat{y} = R$ into the definition of the similarity variable in Eq. (A3), we obtain an expression for the entrance length,

$$\hat{\ell} = R^{\frac{\alpha+1}{\alpha}} \frac{\rho V^{\frac{2\alpha-1}{\alpha}}}{\alpha\kappa\, g(\alpha)^{(\alpha+1)/\alpha}}. \tag{A4}$$

Using the normalization introduced in Eq. (22) and assuming that $V = \hat{\dot{h}}$, the normalized entrance length, $\ell = \hat{\ell}/h_0$, is given by

$$\ell = \frac{8^{1/\alpha}}{\alpha\, g(\alpha)^{(\alpha+1)/\alpha}} \frac{\dot{h}^{\frac{2\alpha-1}{\alpha}}}{\mathrm{Ri}\,\mathrm{El}^{(\alpha-1)/\alpha}}. \tag{A5}$$

Such a relation can be used to estimate the boundary layer growth in regimes where the shear-thinning effect dominates over the zero-shear-rate effect. Figure 8(b) shows the evolution of both the column height and the entrance length calculated by Eq. (A5). Similarly to what is observed in the Newtonian limit discussed before, when the Richardson number is sufficiently high, ℓ is comparable to the column height only at very early times, and its contribution to the imbibition dynamics is negligible. Only when Ri assumes values lower than unity, the boundary layer growth cannot be neglected.

To sum up, since the model presented in this work neglects the boundary layer growth at the tube entrance, its applicability is restricted to regimes where the Richardson number is greater than the unity. This allow us to study both the Lucas-Washburn regime (i.e., $\mathrm{Ri} \to \infty$) and the transition to the inertial oscillatory regime for $\mathrm{Ri} \geqslant 1$.

2. Velocity shape factors

The shape factor defined in Eq. (10) is a function of time via the variable P, the Ellis number, and the shear-thinning index, i.e., $\gamma = \gamma(P(t), \mathrm{El}, \alpha)$, and it is given by

$$\gamma = \frac{(\alpha+3)\left\{4(5+\alpha)\left(\frac{|P|}{\mathrm{El}}\right)^{2\alpha} + 4^{\alpha}(\alpha+2)\left[2^{-\alpha}(\alpha+7)\left(\frac{|P|}{\mathrm{El}}\right)^{\alpha+1} + \frac{(5+\alpha)(\alpha+3)}{12}\left(\frac{|P|}{\mathrm{El}}\right)^{2}\right]\right\}}{4(5+\alpha)(2+\alpha)\left[\left(\frac{|P|}{\mathrm{El}}\right)^{\alpha} + \frac{|P|}{\mathrm{El}}\frac{2^{\alpha}(\alpha+3)}{8}\right]^{2}}. \tag{A6}$$

The evolution of the shape factor as a function of the column speed, $\dot{h}$, and the Ellis number, El, is given in Fig. 10(a). In the proximity of $P = 0$, the shape factor reaches the Newtonian limit of 4/3. Given the analytical expression, we can evaluate the time derivative of the shape factor using the chain rule for derivatives

$$\frac{d\gamma(t, \mathrm{El}, \alpha)}{dt} = \gamma'(\dot{h}, \mathrm{El}, \alpha)\ddot{h}, \tag{A7}$$

where

$$\gamma'(\dot{h}, \mathrm{El}, \alpha) = \frac{\partial\gamma}{\partial P}\frac{\partial P}{\partial\dot{h}}. \tag{A8}$$

The derivative $\partial\gamma/\partial P$ can be obtained analytically using a symbolic calculator from Eq. (A6) while $\partial P/\partial\dot{h}$ is obtained from

$$\frac{\partial P}{\partial\dot{h}} = \frac{1}{\partial\dot{h}/\partial P}, \tag{A9}$$

taking the expression of the column speed from Eq. (25). The evolution of the product $\dot{h}\gamma'$ as a function of the column speed, $\dot{h}$, and the Ellis number, El, is given in Fig. 10(b). In the proximity of $P = 0$, the product reaches the Newtonian limit of zero.

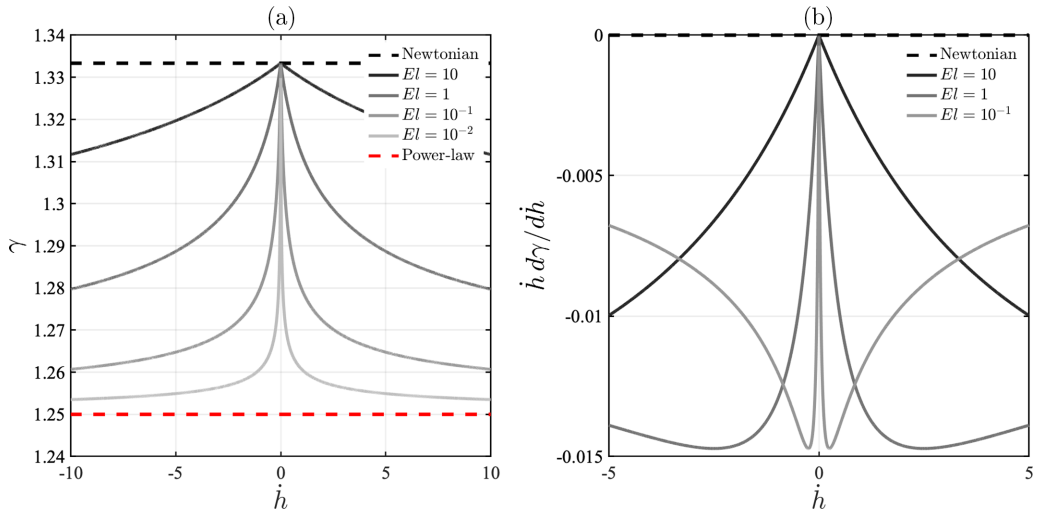

FIG. 10. (a) Evolution of the shape factor, γ, as a function of the column speed for different El and $\alpha = 2$. (b) Evolution of the product $\dot{h}\gamma$ as a function of the column speed for different El and $\alpha = 2$.

3. Jacobian in the Newtonian limit

The Jacobian of the system described in Eq. (35) evaluated at the equilibrium in the limit of El $\to \infty$ where the shape factor reaches a constant value $\gamma = 4/3$, $\gamma' = \gamma'' = 0$, the pressure gradient is linear with respect to the averaged velocity, $P = -\dot{h}$, is given by

$$\boldsymbol{J}(\boldsymbol{x}_0) = \begin{pmatrix} \frac{\partial f_1}{\partial \dot{h}}\Big|_0 & \frac{\partial f_1}{\partial h}\Big|_0 \\ \frac{\partial f_2}{\partial \dot{h}}\Big|_0 & \frac{\partial f_2}{\partial h}\Big|_0 \end{pmatrix} = \begin{pmatrix} -\frac{6\mathrm{Ri}}{7\mathrm{Bo}+8} & -\frac{6\mathrm{Ri}}{7\mathrm{Bo}+8} \\ 1 & 0 \end{pmatrix}. \tag{A10}$$

4. Power-law limit

The model valid in the limit of Bo $\ll 1$, Eq. (29), can be easily derived also for the case of a power-law fluid yielding to

$$\frac{1}{\mathrm{Ri}}\left[\ddot{h}\left(\frac{\alpha+3}{\alpha+2}h + \frac{7}{6}\mathrm{Bo}\right) + \frac{\alpha+3}{2\alpha+4}\dot{h}^2\right] + h = 1 - \mathrm{sgn}(\dot{h})\, h\, \dot{h}^{\frac{1}{\alpha}} \left[\frac{(\alpha+3)(2\mathrm{El})^{\alpha-1}}{4}\right]^{\frac{1}{\alpha}}, \tag{A11}$$

where the shape factor can be written in closed form as $\gamma = (\alpha+3)/(\alpha+2)$ and the dimensionless pressure gradient is given by

$$P = \left[\mathrm{sgn}(\dot{h})\frac{(\alpha+3)(2\mathrm{El})^{\alpha-1}}{4}\dot{h}\right]^{\frac{1}{\alpha}}. \tag{A12}$$

The calculation of the Jacobian of the system in the power-law limit, Eq. (A11), evaluated at the equilibrium reads

$$\boldsymbol{J}(\boldsymbol{x}_0) = \begin{pmatrix} 0 & -\frac{6\mathrm{Ri}(\alpha+2)}{(7\mathrm{Bo}+6)\alpha+14\mathrm{Bo}+18} \\ 1 & 0 \end{pmatrix}. \tag{A13}$$

By inspection of the Jacobian of the linearized system, we can see that the characteristic equation admits only imaginary solutions revealing that the system behaves like an undamped oscillator and oscillate for an infinite time [44]. In this case, the system behaves like a mass-spring system where the damping mechanism is set to zero.

[1] T. C. Chao, O. Arjmandi-Tash, D. B. Das, and V. M. Starov, Spreading of blood drops over dry porous substrate: Complete wetting case, J. Colloid Interface Sci. **446**, 218 (2015).
[2] B. G. Swanson, J. S. Hughes, and H. P. Rasmussen, Seed Microstructure: Review of Water Imbibition in Legumes, Food Struct. **4**, 115 (1985).
[3] Q. Meng, H. Liu, J. Wang, and H. Zhang, Effect of wetting-phase viscosity on cocurrent spontaneous imbibition, Energy Fuels **30**, 835 (2016).
[4] R. Lucas, Ueber das zeitgesetz des kapillaren aufstiegs von flüssigkeiten, Kolloid-Z. **23**, 15 (1918).
[5] E. W. Washburn, The dynamics of capillary flow, Phys. Rev. **17**, 273 (1921).
[6] N. R. Tas, J. Haneveld, H. V. Jansen, M. Elwenspoek, and A. van den Berg, Capillary filling speed of water in nanochannels, Appl. Phys. Lett. **85**, 3274 (2004).
[7] A. Han, G. Mondin, N. G. Hegelbach, N. F. de Rooij, and U. Staufer, Filling kinetics of liquids in nanochannels as narrow as 27 nm by capillary force, J. Colloid Interface Sci. **293**, 151 (2006).
[8] J. Szekely, A. W. Neumann, and Y. K. Chuang, The rate of capillary penetration and the applicability of the Washburn equation, J. Colloid Interface Sci. **35**, 273 (1971).
[9] D. Quéré, Inertial capillarity, Europhys. Lett. **39**, 533 (1997).
[10] M. D. N. Fries, The transition from inertial to viscous flow in capillary rise, J. Colloid Interface Sci. **327**, 125 (2008).
[11] S. Das and S. K. Mitra, Different regimes in vertical capillary filling, Phys. Rev. E **87**, 063005 (2013).
[12] M. Bracke, F. De Voeght, and P. Joos, The kinetics of wetting: The dynamic contact angle, in *Trends in Colloid and Interface Science III*, edited by P. Bothorel and E. J. Dufourc (Steinkopff, Darmstadt, 1989), pp. 142–149.
[13] Ruiz-Gutierrez, Elfego, S. Armstrong, S. Leveque, C. Michel, I. Pagonabarraga, G. G. Wells, A. Hernandez-Machado, and R. Ledesma-Aguilar, The long cross-over dynamics of capillary imbibition, J. Fluid Mech. **939**, A39 (2022).
[14] F. Maggi and F. Alonso-Marroquin, Multiphase capillary flows, Int. J. Multiphase Flow **42**, 62 (2012).
[15] H. Lim, A. Tripathi, and J. Lee, Dynamics of a capillary invasion in a closed-end capillary, Langmuir **30**, 9390 (2014).
[16] B. V. Zhmud, F. Tiberg, and K. Hallstensso, Dynamics of capillary rise, J. Colloid Interface Sci. **228**, 263 (2000).
[17] A. Salama, Investigation of the imbibition/drainage of two immiscible fluids in capillaries with arbitrary axisymmetric cross-sections: A generalized model, J. Fluid Mech. **947**, A12 (2022).
[18] R. Bird, R. Armstrong, and O. Hassager, *Dynamics of Polymeric Liquids Vol 1: Fluid Mechanics* (John Wiley and Sons, New York, NY, 1987).
[19] C. L. A. Berli and R. Urteaga, Asymmetric capillary filling of non-Newtonian power law fluids, Microfluid. Nanofluid. **17**, 1079 (2014).
[20] N. Srivastava and M. A. Burns, Analysis of non-Newtonian liquids using a microfluidic capillary viscometer, Anal. Chem. **78**, 1690 (2006).
[21] R. M. Digilov, Capillary rise of a non-Newtonian power law liquid: Impact of the fluid rheology and dynamic contact angle, Langmuir **24**, 13663 (2008).
[22] F. Shan, Z. Chai, and B. Shi, A theoretical study on the capillary rise of non-Newtonian power-law fluids, Appl. Math. Model. **81**, 768 (2020).
[23] S. R. Gorthi, S. K. Meher, G. Biswas, and P. K. Mondal, Capillary imbibition of non-Newtonian fluids in a microfluidic channel: Analysis and experiments, Proc. R. Soc. A **476**, 20200496 (2020).
[24] D. Picchi, P. Poesio, A. Ullmann, and N. Brauner, Characteristics of stratified flows of Newtonian/non-Newtonian shear-thinning fluids, Int. J. Multiphase Flow **97**, 109 (2017).
[25] D. Picchi, A. Ullmann, N. Brauner, and P. Poesio, Motion of a confined bubble in a shear-thinning liquid, J. Fluid Mech. **918**, A7 (2021).
[26] H. A. S. Evgeniy Boyko, Flow rate-pressure drop relation for shear-thinning fluids in narrow channels: Approximate solutions and comparison with experiments, J. Fluid Mech. **923**, R5 (2021).
[27] A. Aquino, D. Picchi, and P. Poesio, Dynamics of a Taylor bubble through a shear-thinning fluid up to finite capillary numbers, J. Non-Newtonian Fluid Mech. **314**, 105003 (2023).
[28] M. Reiner, *Deformation, Strain, and Flow* (Interscience, New York, NY, 1965), p. 246.

[29] P. J. Carreau, Rheological equations from molecular network theories, Trans. Soc. Rheol. **16**, 99 (1972).
[30] S. Girardo, S. Palpacelli, A. D. Maio, R. Cingolani, S. Succi, and D. Pisignano, Interplay between shape and roughness in early-stage microcapillary imbibition, Langmuir **28**, 2596 (2012).
[31] R. Sousa, M. Riethmuller, A. Pinto, and J. Campos, Flow around individual Taylor bubbles rising in stagnant CMC solutions: PIV measurements, Chem. Eng. Sci. **60**, 1859 (2005).
[32] A. A. Duarte, D. E. Strier, and D. H. Zanette, The rise of a liquid in a capillary tube revisited: A hydrodynamical approach, Am. J. Phys. **64**, 413 (1996).
[33] P. R. Waghmare and S. K. Mitra, Finite reservoir effect on capillary flow of microbead suspension in rectangular microchannels, J. Colloid Interface Sci. **351**, 561 (2010).
[34] A. Budaraju, J. Phirani, S. Kondaraju, and S. S. Bahga, Capillary displacement of viscous liquids in geometries with axial variations, Langmuir **32**, 10513 (2016).
[35] A. Salama, J. Kou, A. Alyan, and M. M. Husein, Capillary-driven ejection of a droplet from a micropore into a channel: A theoretical model and a computational fluid dynamics verification, Langmuir **38**, 4461 (2022).
[36] V. E. B. Dussan, Hydrodynamic stability and instability of fluid systems with interfaces, Arch. Ration. Mech. Anal. **57**, 363 (1975).
[37] R. G. Cox, The dynamics of the spreading of liquids on a solid surface. Part 1. Viscous flow, J. Fluid Mech. **168**, 169 (1986).
[38] O. Voinov, Hydrodynamics of wetting, Fluid Dyn. **11**, 714 (1976).
[39] P. Neogi and R. M. Ybarra, The absence of a rheological effect on the spreading of small drops, J. Chem. Phys. **115**, 7811 (2001).
[40] F. M. White, *Fluid Mechanics*, 6th ed., McGraw-Hill Series in Mechanical Engineering (McGraw-Hill, New York, NY, 2009).
[41] A. Acrivos, M. J. Shah, and E. E. Petersen, Momentum and heat transfer in laminar boundary-layer flows of non-Newtonian fluids past external surfaces, AIChE J. **6**, 312 (1960).
[42] W. R. Schowalter, The application of boundary-layer theory to power-law pseudoplastic fluids: Similar solutions, AIChE J. **6**, 24 (1960).
[43] J. P. Denier and P. P. Dabrowski, On the boundary-layer equations for power-law fluids, Proc. R. Soc. London A **460**, 3143 (2004).
[44] M. C. de Oliveira, *Fundamentals of Linear Control: A Concise Approach* (Cambridge University Press, Cambridge, UK, 2017).